*- Technical Paper -*

# STUDY ON BENDING BEHAVIOR OF HOLLOW SEGMENTAL CIRCULAR UFC BEAMS PRESTRESSED WITH UNGROUTED PC BARS

Mamy A. RABOTOVAO[*1] and Tomohiro MIKI[*2]

ABSTRACT

The structural integrity of precast concrete components mainly depends on the connections between the precast structural elements. In this paper, different interface types and parameters representing the epoxy joint were considered to observe the effect of those epoxy joints on the behavior of precast concrete (PCa) and ultra-high strength fiber reinforced concrete (UFC) hollow circular segmental PC beams. This study reports how the quality of connections affects the load bearing capacity and the failure mechanism of such structure. A weak interface will lead to a reduction of flexural stiffness and the stress transfer of in the concrete body of the specimens.

Keywords: Segmental beams, Ultra High Strength Reinforced Fiber concrete (UFC), Prestressed Ungrouted PC bars, FEM

## 1. INTRODUCTION

Precast construction, also known as prefabricated construction, includes those bridges and buildings where most of the structural components are standardized and produced in plants in a location away from the construction and then transported to the site for assembly. The structural components are manufactured by industrial methods based on mass production to build many buildings in a short time at a low cost. The most frequently used types of precast concrete elements are columns, beams, hollow-core slabs, pocket foundations. The use of precast products is regarded in the construction standards as an advantage that helps to reduce some of the coefficients used in design, but there are other specific advantages of precasting that are easily noticed on site.

The precast concrete (PCa) component is mainly assembled with the use of joints and prestressing force. For precast prestressed concrete structures, connection can be a critical challenge since they play a significant role in controlling the behavior of structures. The performance of those structures is greatly influenced by the connection modes.

In recent years, PCa segmental bridges with hybrid tendons and epoxy joints become increasingly popular. PCa segmental bridges with hybrid tendons and dry joints are thought to be a competitive alternative for rapid construction. However, due to the stress concentration at the dry joints, the ultimate strength of segments with dry joints could be less than that with epoxy joints [1]. The epoxy joints possess a higher shear-resistance capacity and better durability than dry joints. In addition, the epoxy resin as a lubricant can mitigate the fixing imperfections between the segmented surfaces [2]. Epoxy joints should be designed to have sufficient capacity to transfer shear force, axial force, and bending moments under static and dynamic loading [3].

Zheng et al. [4] have modeled the epoxy joint between PCa UFC segmental beam as a surface-to-surface interaction with two contact properties including two types: normal behavior and shear behavior. A hard contact type was adopted as normal behavior, in other words the amount of stress transfer in the interface was not limited. For shear behavior a Coulomb friction model with a friction coefficient of 0.7 was adopted. In both normal behavior and shear behavior model, when the pressure in the interface was zero or negative, the two contact surfaces split. Author concluded on the fact that numerical simulation analysis of large sized PCa UFC segmental beams requires the investigation on more interface parameters to understand the flexural load capacity of those members [4].

Some research investigated the load carrying capacity of PCa ultra-high strength fiber reinforced concrete (UFC) segmental hollow circular beams however it lacks investigation on understanding the effect of the joint (interface) between the segmental components on the load carrying capacity, the stress distribution and the cracking pattern. To solve the issue, in this study, different interface types and parameters representing the epoxy joint were considered to observe the effect of those epoxy joints on the behavior of PCa UFC hollow circular segmental PC beams.

## 2. ANALYTICAL METHODS

### 2.1 Analysis Targets

This study aims at reproducing an experiment [5] that was carried out on a UFC segmental hollow circular beam with DIANA 10.7. The beam was composed of 5 segments bonded to each other with resin. This analytical study aimed at reproducing that experiment. Analytical specimens consisted of hollow circular UFC beam with an external diameter of 1000 mm and a thickness of 70 mm. Each specimen has a length of 10 meters. Regarding the design of the specimens, monolithic and segmental.

Table 1 shows the details of all analytical specimens. In the designation part S or M represent whether the specimen is segmental or monolithic, E and NE mean elastic interface and non-elastic interface, the letters 1 or 2 mentioned the type of

*1 PhD student, Dept. of Civil Engineering, Kobe University, JCI Student Member
*2 Associate Prof., Dept. of Civil Engineering, Kobe University, Dr.Eng., JCI Member

Table 1 Specimens details

| Type of specimen | Designation | Length (m) | Thickness (mm) | Prestress (N/mm$^2$) |
|---|---|---|---|---|
| Segmental | Exp. [5] | 10 | 70 | 8.54 |
| Monolithic | M-8 | 10 | 70 | 8.54 |
| Segmental | S-E1-8 | 10 | 70 | 8.54 |
| | S-E2-8 | 10 | 70 | 8.54 |
| | S-NE1-8 | 10 | 70 | 8.54 |
| | S-NE2-8 | 10 | 70 | 8.54 |
| | S-NE1-12 | 10 | 70 | 12 |
| | S-NE2-12 | 10 | 70 | 12 |
| | S-NE1-4 | 10 | 70 | 4 |
| | S-NE2-4 | 10 | 70 | 4 |

interface used for the interfaces explained next section, and the last digits 8 or 12 or 4 represent the level of prestress in the concrete.

## 2.2 Modeling

(1) Geometry and meshing of specimens

Figure 1 shows the geometry and meshing of specimens with a mesh size of 50 mm. Figure 2 shows the details of the supports. Two lines were drawn at the bottom faces of both supports (support left and right). The left support of the beam was fixed in all directions X, Y and Z on that line. The right support was only fixed in two direction Y and Z. Moreover, it is suggested that the displacement along of Y axis of the bottom faces of both supports is fixed as well as the rotation of those faces around X and Z direction (this is done so that the support plates marry the movement of the beam during the loading). Disposition of PC bars are shown in Fig.3. Each specimen was reinforced with 18 PC bars.

(2) Constitutive models of UFC [6]

The total based cracked model is considered to model the UFC concrete. The measured modulus of elasticity of UFC during experiment is 46000 N/mm$^2$. The compressive strain-stress curve for UFC is shown by Fig.4(a) The measured compressive strength was 180 N/mm$^2$, so in the analysis the compressive strength was taken as 153 N/mm$^2$, the measured tensile strength of UFC concrete was 8.8 N/mm$^2$. UFC tensile model was modelled as shown by Fig.4(b) with $\varepsilon_{cr}, \varepsilon_1$ and $\varepsilon_2$ are 0.0001913, 0.013 and 0.109 respectively.

(3) PC bars (tendons)

PC bars are the only reinforcement in the UFC structure. The elastic modulus was 200000 N/mm$^2$ and the yielding stress was 1175 N/mm$^2$. In this paper, PC bars are modelled as bond slip reinforcement with a very weak bond slip between the UFC concrete and PC bars. Bond slip parameters are detailed in the section 2.3. In this case, weak bond slip interface refers to a very low normal stiffness and shear stiffness moduli.

(4) Interface element

The interface represents the joint between two segments of the beam. A surface-to-surface interface element was used. This surface-to-surface interface element is a typical model of the interface between two touched solid elements. Normal and shear stiffnesses values were assigned to these surfaces. Element local x-axis in the local coordinate system is the first node pointing to the second one on the surfaces of contacted solid elements and the y-axis is in the normal direction. Element z-axis is perpendicular to plane co-determined by the x and y coordinate axes, which is also the outer-plane direction perpendicular to element plane. Regarding the parameters of the

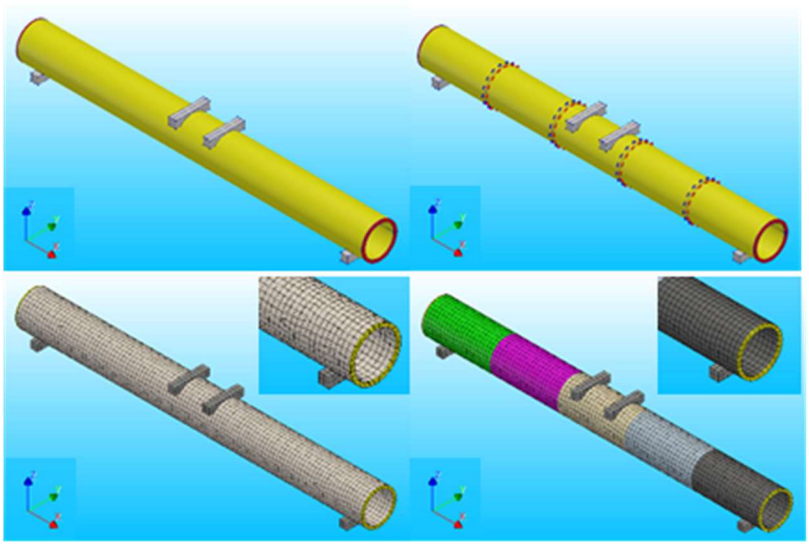

(a) Monolithic model (b) Segmental model

Fig.1 Geometry and meshing of specimens

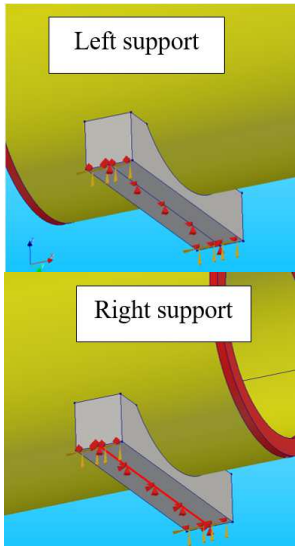


Fig.2 Detail of supports

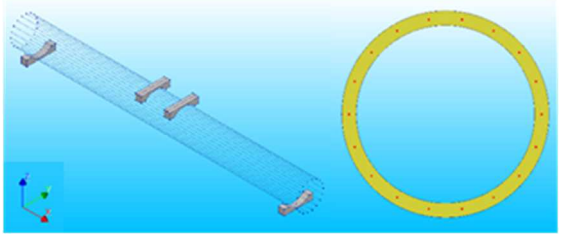

Fig.3 PC bars

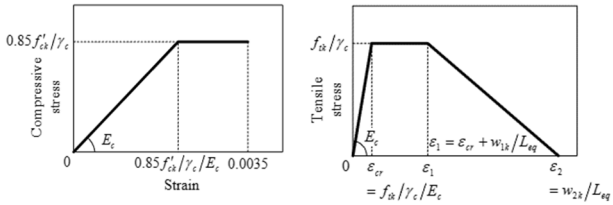


(a) Compressive model (b) Tensile model

Fig.4 Constitutive models of UFC

Table 2 Interface parameters representing the joint between two segments.

| Type | ID | Shear and normal stiffness ($N/mm^3$) | Critical opening (mm) | Normal stiffness reduction factor |
|---|---|---|---|---|
| Linear | E1 | 10000 | - | - |
| Linear | E2 | 100 | - | - |
| Non-linear | NE1 | 10000 | 0.001 | 0.001 |
| Non-linear | NE2 | 100 | 0.001 | 0.001 |

surface interface element used to represent the joint between two segments. As shown by Table 2, normal and shear stiffness moduli of the surface-to-surface interface were the same for all cases. Using a shear stiffness modulus 1000 times smaller than the normal stiffness led to large sliding of the segments of the beam, therefore the bending behavior of the beam could not be observed. The value 100 $N/mm^3$ were selected among different values to be shown in this paper since it shows similar values of opening of epoxy joint as it was observed in the experiment [5]. The value of 10000 $N/mm^3$ was an exaggerated value of stiffness modulus. The critical opening of 0.001 mm was considered since a high value of critical opening tends to premature the failing of specimens. A normal stiffness reduction of 0.001 was set since all tried normal stiffness reduction factors (0.1, 0.05, 0.01, …) higher than that value will not affect the failure pattern of the specimens.

### 2.3 Post-tensioning process

The post-tensioning process can be a challenging task to reproduce in the analysis. To do so, phased analysis was used. Two phases are represented as the jacking phase and the locking phase as follows.

1. The jacking phase: during this phase, jacking force is applied to all the PC bars at the same time. Specimens do not present any anchor plates and loading plates at this stage. To reproduce the no contact between UFC and PC bars, a normal stiffness modulus of 1000 $N/mm^3$ and a shear stiffness modulus of 0.2 $N/mm^3$ are considered as bond bond-slip parameters between them. Moreover, in this phase, the PC bars were associated with a Shima bond-slip curve but to represent the void between PC bars and UFC, the compressive strength of concrete in the Shima bond slip [7] equation is taken as 0.001 $N/mm^2$. The compressive strength of 0.001 $N/mm^2$ is DIANA's recommendation in reproducing post tensioned structural member.
2. The locking phase: during this phase, the anchor plates and loading plates were set in the analysis. Moreover, tyings were added to fix PC bars to the anchor plates. Tyings are linear dependences between nodal variables that are defined in geometry and passed to the mesh, used to restrain the displacement of the anchor points. After this stage the loading was carried out. A normal stiffness modulus of 1000 $N/mm^3$ and a shear stiffness modulus of 0.2 $N/mm^3$ were considered bond-slip parameters. With the assumption that PC bars and UFC, despite the ungrouted case, will be in contact at certain stage of the loading due to the bending of the beam.

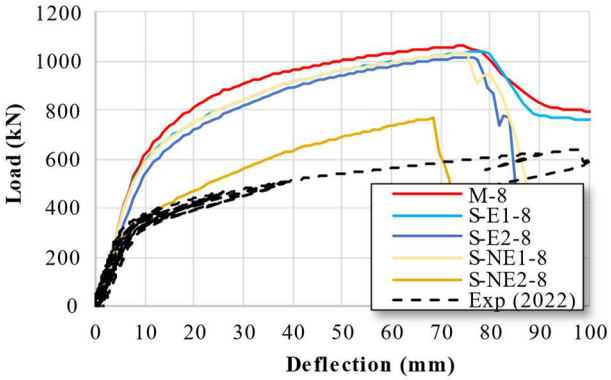


Fig.5 Effect of the interface parameter on the load deflection curves.

## 3. ANALYSIS FOR EFFECTS OF INTERFACE

This section reports the experiment and analytical results for a designed prestressed level of 8 $N/mm^2$ in the concrete. This corresponds to a prestressing force of 100 kN for each PC bar.

(1) Load carrying capacity.

Figure 5 shows both experimental and analytical results. The deflection was measured at the midspan for all the specimens whether experimental or analytical. As shown in Fig.5, the experimental specimen's load deflection curve presents two different flexural stiffnesses. As it reached a load of 300 kN, the change in flexural stiffness was evident. This second flexural stiffness was kept constant until the failure happened at the loading of 637 kN.

Regarding the analytical specimens, it is observed that specimen M-8 can reach a load-carrying capacity of 1060 kN. At a deflection of 80 mm, the monolithic specimen shows a loss of bearing capacity, however, no failure of the specimen was observed.

Analytical specimens with an elastic interface parameter, S-E1-8, and S-E2-8 present respectively the load-carrying capacities of 1037 kN and 1015 kN, respectively. The huge difference between these two specimens was that after reaching a peak load, specimen S-E1-8 presented just a loss of bearing capacity as the monolithic specimen, however, specimen S-E2-8 presented a sudden drop of carrying capacity representative of its failure.

Regarding the specimens S-NE1-8 and S-NE2-8, those specimens reached maximum loads of 1034 kN and 768 kN respectively. The specimen S-NE1-8 presents a load deflection like all previous analytical specimens, which can be described as an initial flexural stiffness similar to the experiment results followed by a gradual decrease in flexural stiffness until maximum load is reached. However, the specimens S-NE2-8 presented almost the same behavior as the experimental results. The difference in second stiffness between the specimen S-NE2-8 and the experimental specimen is due to the larger contribution of the PC bars. This larger contribution of PC bars is caused by some limitation on reproducing the ungrouted situation with DIANA ver 10.7. For this specimen, the failure occurred at a lower deflection of 65 mm and with a load carrying capacity of 768 kN, however, after the initial flexural stiffness the sudden change in stiffness was also observed as it is in the experiment.

(2) Cracking patterns

It is reported that the experimental specimen presents large cracks at both joints located in the middle. Those cracks

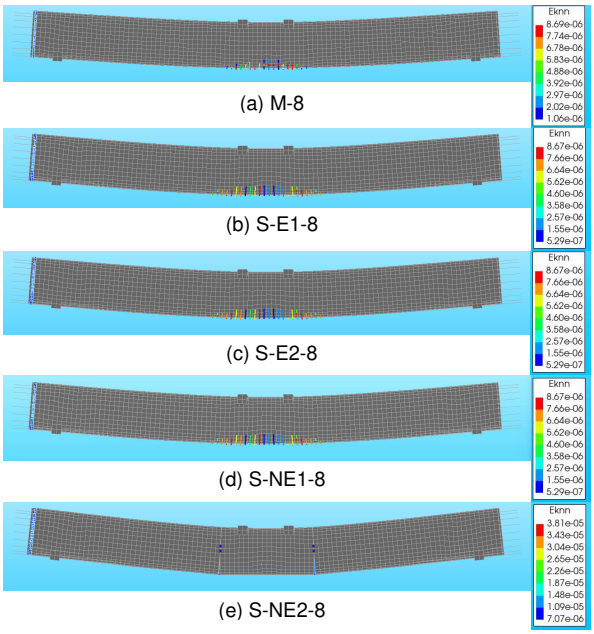


Fig.6 Cracking patterns at P = 345 kN

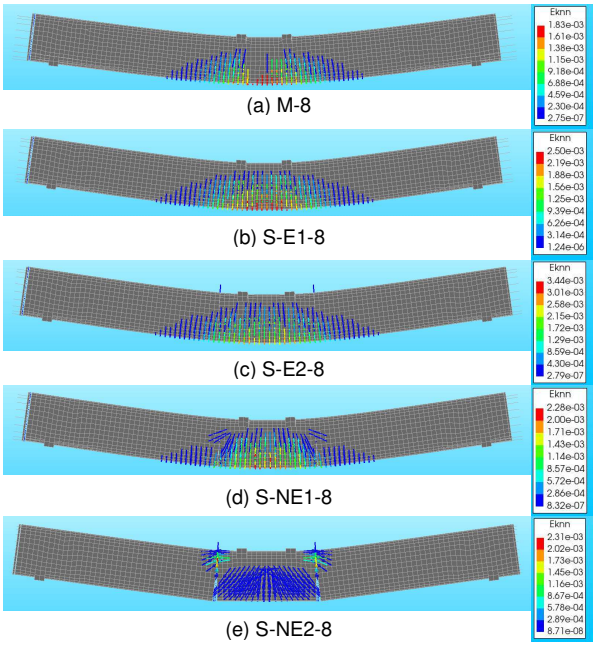


Fig.7 Cracking patterns at P = 750 kN

propagate along the joint from the bottom to the neutral axis of the beam, up to the failure of the specimen. To analyze the cracking patterns of analytical specimens, two different loading stages are considered: 345 kN and 750 kN. The first loading of 345 kN corresponds to the crack opening of all the specimens. The second loading is taken to understand the crack propagation of all the specimens. This section reports the $E_{knn}$ (normal concrete cracking strain in the integration point).

The crack starts opening at a loading of 345 kN for all analytical cases. As shown in Fig.6, all the specimens present flexural cracks. Regarding those cracking patterns, except for specimen S-NE-8, all segmental specimens present more intervals than the monolithic specimen. The crack strain of the specimens at this stage is almost similar. Specimen S-NE2-8 on the other hand, presents no flexural cracks but instead shows a large opening of the interfaces located in the middle segment of the beam.

Table 3 Tensile strain in the PC bars

| | Tensile strain in the PC bars ($\mu$) |
|---|---|
| Exp. [5] | 6190 |
| M-8 | 18250 |
| S-E1-8 | 15490 |
| S-E2-8 | 8940 |
| S-NE1-8 | 14210 |
| S-NE2-8 | 7590 |

Table 4 Opening of the interfaces in the middle of the beams

| | Opening at P=345 kN (mm) | Opening at peak load (mm) |
|---|---|---|
| S-E1-8 | 0.0008 | 0.001 |
| S-E2-8 | 0.09 | 0.1 |
| S-NE1-8 | 0.0008 | 0.94 |
| S-NE2-8 | 1.52 | 17 |

The crack distribution of analytical specimens for a load of 750 kN is shown in Fig.7. This loading level was considered since the peak load specimen S-NE-8 was only 768 kN. As shown in Fig.7, more flexural cracks are observed for specimens M-8, S-E1-8 and S-E2-8. However, the monolithic specimen M-8 shows less interval of cracks than the other two. Moreover, at this stage, the specimen M-8 shows only an $E_{knn}$ of 0.00183 although the other specimens show $E_{knn}$ of 0.0025 and 0.0034 respectively for S-E1-8 and S-E2-8. In the case of S-E2-8, small cracks are observed in the top part of the beam.

For specimen S-NE1-8, several flexural cracks are observed along with some cracks presenting different angles just under the two loading points. In the case of specimen S-NE2-8, all the flexural cracks are concentrated in the middle segments of the beam. Moreover, a concentration of horizontal cracks was observed in the top part of the interface located in the middle of the beam.

(3) Tensile strain in PC bars

This section presents the tensile strain in the PC bars located in the tensile zone of the beam. Table 3 provides the tensile strain in the PC bars for different specimens. As seen in Table 3, none of the PC bars has reached the ultimate tensile strain of 30000$\mu$. Those measurements were taken at the mid-span of the beam. The tensile strain in the PC bar was obtained directly under the location of the loading. Since during the experiment, the initial measurement was carried out after completion of the post tensioning, a tensile strain of 3770$\mu$ (tensile strain generated by the jacking process of the PC bars) was added to the tensile strain of PC bar at the peak load of the experimental result.

(4) Opening of the interfaces

The opening of the analytical specimens at the same location as the experiment is shown in the Table 4. During experiment loading test, the joint next to the right loading plate presents the following opening at its bottom part, an opening displacement of 0.38 mm for a load of 345 kN and that of 25.4 mm at the peak load of 637.2 kN.

(5) Failure mechanism

All specimens show different failure patterns as shown by Fig.8. The specimens M-8, S-E1-8 ad S-NE1-8 show a large flexural crack in the middle of the beam. All those three specimens show a bending failure. Specimen S-E2-8 also showed a bending failure but on the other hand two large flexural

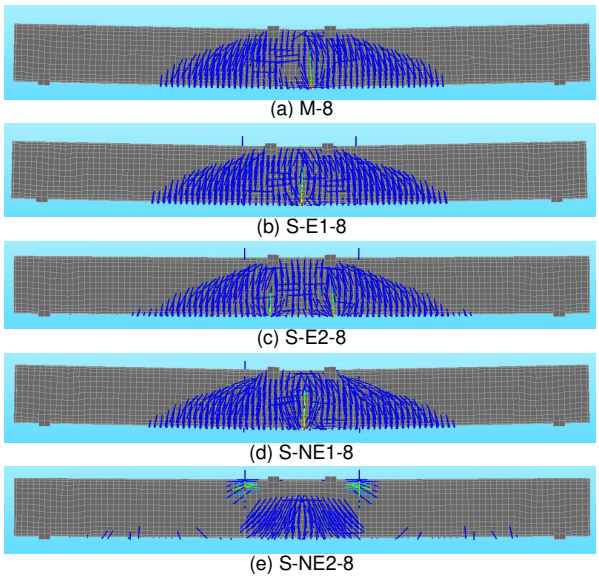


Fig.8 Failure patterns

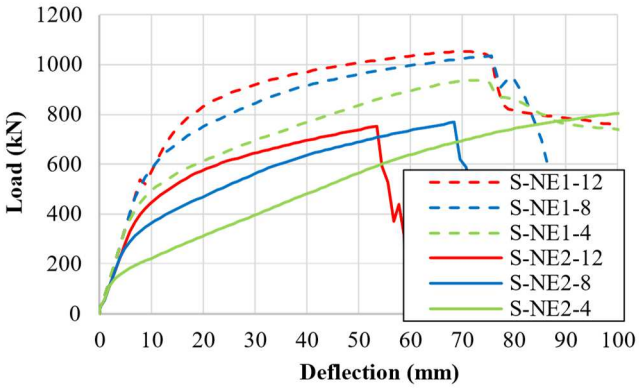


Fig.9 Effect of the prestressing level on the load deflection curves of specimens

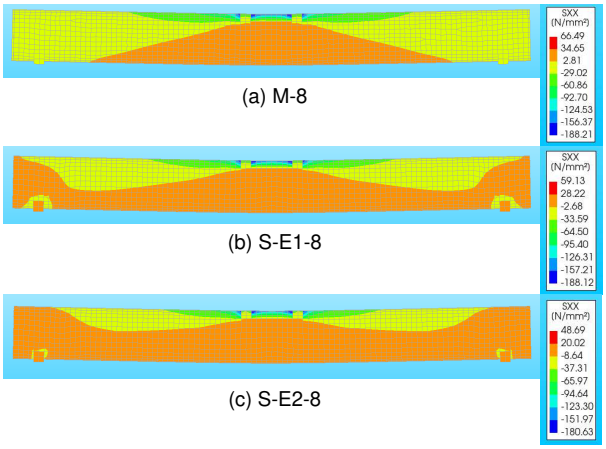


Fig.10 Stress distribution of specimens with linear interfaces

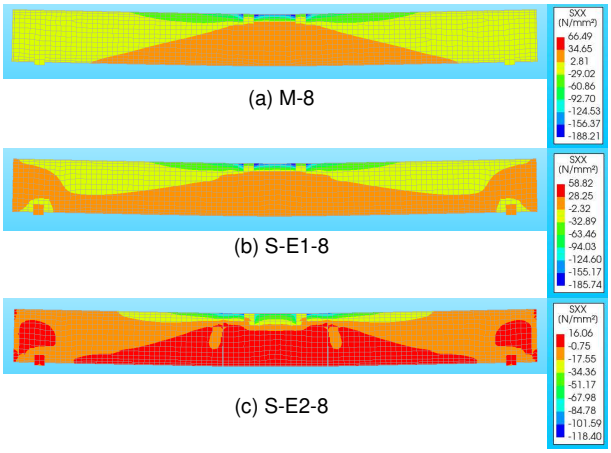


Fig.11 Stress distribution of specimens with non-linear interfaces

cracks were observed just under the location of the loading point. For the last specimen S-NE2-8, a concentration of flexural cracks is observed in the middle segments of the beam followed by large horizontal cracks on the top part of that segment.

## 4. EFFECT OF PRESTRESSING LEVEL ON THE LOAD CARRYING CAPACITY OF SPECIMENS.

This section presents the effects of different magnitudes of prestress in the concrete on the bending behavior of UFC segmental beams. Three different levels of prestress in the concrete are considered; 4 N/mm$^2$, 8 N/mm$^2$ and 12 N/mm$^2$, respectively.

Figure 9 shows the load deflection curves of specimens with different prestressing levels. By comparing the specimens S-NE1-12, S-NE1-8 and S-NE1-4, it can be seen that the increase in the magnitude of the prestress in concrete increases the second flexural stiffness of the specimens. On the other hand, S-NE1-12 and S-NE1-8 present similar load carrying capacities of 1050 kN and 1034 kN respectively. All those three specimens present the same deflections at the peak load.

For specimens S-NE2-12 and S-NE2-8, those specimens present different load carrying capacities of 752 kN and 768 kN respectively. Moreover, those peak loads are reached at a very low deflection of 55 mm and 68 mm for S-NE2-12 and S-NE2-8 respectively. On the other hand, S-NE2-4 presents no failure yet at a deflection of 100 mm, with a loading of 800 kN.

## 5. DISCUSSIONS

The existence of the joints should prevent any cracking in the body of the concrete with their opening. However, analysis shows that cracking of concrete appears at the location of the interface in the mid-span. In this research, the main parameters were set as the surface interface conditions.

Modelling the interface with linear parameters leads to almost the same load carrying capacities as the monolithic one as shown in Fig.9 for specimens S-E1-8 and S-E2-8. Interfaces E1 and E2 differ regarding their shear and normal stiffness modulus. E1 presents a shear and normal stiffnesses moduli of 10000 N/mm$^3$, while E2 presents only 100 N/mm$^3$. This difference in parameters seems to not affect the load carrying capacity at all, but somehow affect the stress transfer in all the components of the beam itself, and therefore the behavior of the beam.

Figure 10 shows the stress distribution of three specimens at their peak load. Here, SXX is the stress in the X direction, in this case along the longitudinal direction of the beam. As shown in Fig.10 the monolithic specimen shows a normal stress distribution where only a part of the midspan of the beam is in tension. However, the stress distribution of S-E1-8 and S-

E2-8 shows a different behavior. Almost all the parts of the beam were in tension and as the strength of the interface reduces the larger the size of the beam in tension. At the peak load, S-E1-8 presents an opening of 0.001 mm, which is negligible, however, this slight opening manages to swift the behavior of the beam, shifting its resisting part to relatively just a small part of the beam.

Analyzing the results of modelling the interface as non-linear material shows that it affects even more the stress transfer in all the components, as we can see in Table 4, the contribution of the reinforcement reduces for the non-linear cases. The nonlinearity of the interface consists of a critical opening at which the normal stiffness modulus will start reducing while the shear stiffness modulus is kept constant. In this research, a critical opening of 0.001 mm and a reduction factor of 0.001 is considered. The specimen S-NE1-8 shows a similar load carrying capacity as the specimen S-E1-8. At the peak load, specimen S-NE1-8 shows an opening of 0.94 mm but it seems the stress distribution is not affected since S-NE1-8 and S-E1-8 shows the same stress distribution at peak load, as shown in Fig.11. High stiffness interface could be representative of a ductile joint that allows a better stress transfer in the body of concrete.

## 6. CONCLUSIONS

This paper can be summarized as follows:

(1) The experimental specimen shows that in the PCa UFC segmental hollow circular beam the UFC concrete presented less damage than normal concrete beams. The bending led to the opening of the joint but did not affect the body of concrete next to the jointing.

(2) The nature of the interface affected the load bearing capacity of the specimens. Modelling interfaces with linear parameters lead segmental specimens to a load bearing capacity like the monolithic specimen as are the cases of S-E1-8 and S-E2-8 in which E1 was representative of a strong interface with stiffnesses moduli of 10000 N/mm$^3$ and E2 a weak interface with 100 N/mm$^3$. S-E1-8 and S-E2-8 presented an interface opening of 0.001 mm and 0.1 mm respectively at the peak load. Those small opening of interfaces affected the stress distribution in concrete that a large part of the UFC beam is in tension for the cases of S-E1-8 and S-E2-8.

(3) The quality of the connections defines the failure mechanism of the specimen. A strong interface that is high shear and normal stiffness moduli will lead to the same failure mechanism as the monolithic specimen as shown by Fig.8 specimen S-E1-8 and S-NE1-8. For both specimens, the stiffnesses moduli of the interface were 10000 N/mm$^3$, which represent a strong connection. On the other hand, in the case of S-NE1-8, beside those stiffnesses moduli a critical opening and reduction of shear stiffness modulus was set. The non-elastic behavior of the interface affected the flexural stiffness of the specimen and not its failure pattern.

(4) Increasing the prestressing level in concrete from 4 to 12 N/mm$^2$ increases the flexural stiffnesses of all specimens as shown in Fig.9. S-NE1-12 presents a high flexural stiffness than that of S-NE1-8 and S-NE1-4. The same thing is also observed as S-NE2-12 presents a higher flexural stiffness than S-NE2-8 and S-NE2-4. However, associating weak interfaces with high prestressing leads to an early failure of the specimen.

## REFERENCES


[1] Haibo Jiang, Qi Cao, Airong Liu, Tianlong Wang, Yun Qiu., "Flexural behavior of precast concrete segmental beams with hybrid tendons and dry joints." *Construction and Building Materials*, Vol.110, 2016, pp.1-7

[2] Ahmed G.H., Aziz O.Q., "Stresses, deformations and damages of various joints in precast concrete segmental box girder bridges subjected to direct shear loading. " *J Eng Struct*, 206, 11051, 2020

[3] Gopal BA, Hejazi F, Hafezolghorani M, Voo, Y.L., "Shear Strength of Dry and Epoxy Joints for Ultra-High-Performance Fiber-Reinforced Concrete." *ACI Struct Journal*, **117**(1), pp.279-289, 2020.

[4] Zheng, H., Chen, D., Ou, M., Liang, X., Luo, Y., "Flexural Behavior of Precast UHPC Segmental Beams with Unbonded Tendons and Epoxy Resin Joints." *Buildings*, **13**, 1643, 2023

[5] 宮原清, 上山幸雄, 田口拓望, 田中敏嗣, 三木朋広 : 超高強度繊維補強コンクリートを用いた円筒部材の正負交番曲げ試験, 土木学会第 77 回年次学術講演会, 2022

[6] Yuichi Uchida , Junichiro Niwa, Yoshihiro Tanaka and Makoto Katagiri., "Outlines of recommendations for design and construction of ultra-high strength fiber reinforced concrete structures". *JSCE specification*

[7] Shima, H., Chou, L-L., and Okamura, H. "Micro and Macro Models for Bond in Reinforced Concrete". *J. of the Faculty of Engineering, The University of Tokyo* (B) 39, 22 (1987), 133-194